

The moat regimes within 2 + 1 flavor Polyakov-Quark-Meson model

Gaoqing Cao

School of Physics and Astronomy, Sun Yat-sen University, Zhuhai 519088, China

(Dated: April 30, 2025)

To better understand recent predictions on the moat regime of quantum chromodynamics (QCD) matter, this paper extends the previous work within the two-flavor Quark-Meson (QM) model to the more realistic 2+1 flavor Polyakov-Quark-Meson (PQM) model. Mainly, two effects are further taken into account: strange quark and confinement coded through Polyakov loop. Model parameters are chosen to consistently reproduce the pseudo-critical temperature from lattice QCD, $T_C \sim 156$ MeV, and the baryon chemical potential at the critical end point (CEP) from FRG-QCD, $\mu_{B(\text{CEP})} \sim 635$ MeV. It is found that the basic features of moat regimes for σ and π mesons remain similar to those from QM model: Moat regimes cover the region where temperature or baryon chemical potential is large; reentrances occur around the critical baryon chemical potential of chiral transition at zero temperature. Thus, the FRG-QCD results can still not be well understood, especially why the CEP should locate at the entrances of moat regimes for σ and π mesons. Nevertheless, some basic features can be understood qualitatively, and it is consistent that the pole energies are increasing functions of momenta in the whole $T - \mu_B$ plane. The moat regime and pole energy of K mesons are also studied with the features similar.

PACS numbers: 11.30.Qc, 05.30.Fk, 11.30.Hv, 12.20.Ds

I. INTRODUCTION

The states of QCD matter under extreme conditions is one of the oldest yet full of vigour and vitality topics in high energy nuclear physics. It is also the most fundamental question in order to study any thermodynamic properties of any QCD systems. According to low energy nuclear physics [1], the first kind of QCD matter can be attributed to nuclear matter which is extended from heavy nuclei and expected to exist in the circumstance with low temperature and large baryon density, such as neutron stars [2]. Due to the saturation properties, it is well known that the transition from vacuum to symmetric nuclear matter is of first order with the critical baryon chemical potential $\mu_B^c \sim 923$ MeV [3, 4]. In 1974, T.D. Lee and G.C. Wick proposed to generate a new QCD state, now known as "quark gluon plasma", by creating a high temperature circumstance through heavy ion collisions [5]. From both lattice QCD simulations [6, 7] and experimental explorations [8, 9], it is clear that the change from quark gluon plasma to hadronic phase is a crossover at low baryon density with the pseudo-critical temperature $T_C \sim 156$ MeV.

Since 1974, the $T - \mu_B$ phase diagram has been widely studied in chiral effective models, but what we are really sure about it are the regions around μ_B^c and T_C . According to model calculations, there could be two important critical end points (CEPs) in between: one for the gas-liquid transition of nuclear matter at lower temperature and the other for the chiral symmetry breaking and restoration at higher temperature. Recently, the existence and location of the latter are under dense investigations from both theoretical and experimental sides in high energy nuclear physics, refer to Refs. [10, 11]. On the theoretical side, functional renormalization approaches [12–14] predicted the location to be in the re-

gion with $\mu_B = 600 \sim 650$ MeV and $\mu_B/T > 4$, roughly consistent with that from holographic QCD [15] but lying between those from lattice QCD simulations with complex μ_B [16] and finite-size scaling analysis [17]. On the experimental side, a lot of facilities worldwide aim at exploring the CEP by decreasing the colliding energy thus approaching the high temperature and high density region, such as RHIC/STAR in USA, FAIR/CBM in Germany, HIAF/CEE in China, and NICA/MPD in Russia [10, 11].

Under such a trend, it is also important to explore possible exotic phases around the CEP, since the prediction and detection of CEP could be greatly affected and experiments might reach the higher density side of CEP. According to the literatures, the most relevant ones are quarkyonic matter and moat regime. The quarkyonic matter is a quark-baryon coexisting phase where chiral symmetry is restored but confinement remains [18], and had been applied to neutron stars [19–22]. The moat regime of QCD was first discovered by applying functional renormalization group to QCD matter (FRG-QCD) [12], where the wave function renormalization of pions becomes negative near the CEP thus features spatial modulations for the mesonic correlations. Then, the possible signatures of moat regime are studied in great details for heavy ion collisions [23–25], and it was found that particle numbers and their correlations greatly enhance at nonzero momentum by following the feature of spectral function.

Recently, FRG-QCD [26] and Quark-Meson model [27] revisited the moat regime by considering both σ and π correlations and exploring their spectral functions. According to FRG-QCD [26], the moat regimes are induced by particle-hole fluctuations, and the boundaries are consistent with the CEP and chiral crossover line therefrom up to around the temperature $T = 140$ MeV. While, the moat boundaries found in QM model [27] are rather far

away from the chiral transition line except the low temperature parts. Specifically, the feature of reentrance was found around μ_B^c in the QM model, that is, the system exists the moat regime at a lower temperature and then enters it again at a higher temperature.

This work is devoted to understanding the different features of moat regimes found in FRG-QCD and Quark-Meson model by adopting the more realistic 2 + 1 flavor Polyakov-Quark-Meson model. The paper is organized as follows. In Sec. II, we present the whole formalism: the Lagrangian density is given in Sec. II A, the gap equations are derived in Sec. II B, and the static and pole energies of mesons are discussed in Sec. II C with the detailed derivations of the polarization functions reserved

in Appendices A and B. In Sec. III, we show our numerical results: the $T - \mu_B$ phase diagram is illustrated together with the CEPs from literatures in Sec. III A, and the features of moat regimes are studied both numerically and analytically in Sec. III B. Finally, we summarize in Sec. IV.

II. POLYAKOV-QUARK-MESON MODEL

A. The Lagrangian density

In Euclidean space with the metric $g^{\mu\nu} = -\delta_{\mu\nu}$, the Lagrangian density of the renormalizable 2 + 1 flavor Polyakov-Quark-Meson (PQM) model [28] is given by

$$\begin{aligned} \mathcal{L}_{\text{PQM}} = & \bar{\psi} \left[i \not{\partial} - i \gamma^4 \left(i g_s \mathcal{A}^4 + Q_q \mu_Q + \frac{\mu_B}{3} \right) - g_m T^a \left(\sigma_a + i \gamma^5 \pi_a \right) \right] \psi + \text{Tr} \left(\mathcal{D}_\mu^\dagger \phi^\dagger \mathcal{D}^\mu \phi - m_\phi^2 \phi^\dagger \phi \right) \\ & - h_1 [\text{Tr}(\phi^\dagger \phi)]^2 - h_2 \text{Tr}[(\phi^\dagger \phi)^2] + \kappa [\text{Det}(\phi^\dagger) + \text{Det}(\phi)] + c_a \text{Tr} T^a (\phi^\dagger + \phi) - V(L, L^*), \end{aligned} \quad (1)$$

where $\psi(x) = (u(x), d(x), s(x))^T$ denotes the three-flavor quark field with the charge matrix $Q_q = \text{dia}(q_u, q_d, q_s)$, \mathcal{A}^4 denotes the interaction matrix with temporal gluons, and $\phi \equiv T^a(\sigma_a + i \pi_a)$ is the scalar-pseudoscalar field matrix. We will establish a more general formalism than that in Ref. [28] by considering the case with finite temperature T , baryon chemical potential μ_B , and electric chemical potential μ_Q . To conveniently introduce μ_Q into the covariant derivatives for mesons, $\mathcal{D}_\mu = \partial_\mu - Q_m \mu_Q \delta_{\mu 4}$ with Q_m the electric charge matrix, we choose $\sigma_a + i \pi_a$ to be the eigenstates of electric charge with eigenvalues q_m . Correspondingly, the interaction matrices in flavor space are

$$\begin{aligned} T^0 &= \sqrt{\frac{1}{6}} \mathbf{1}, & T^a &= \frac{\lambda^a}{2} \quad (a = 3, 6, 7, 8), \\ T^{1,2} &= \frac{\lambda^1 \mp i \lambda^2}{2\sqrt{2}}, & T^{4,5} &= \frac{\lambda^4 \mp i \lambda^5}{2\sqrt{2}} \end{aligned} \quad (2)$$

with λ^a the Gell-Mann matrices. In the vacuum, u and d quarks are almost degenerate and there is no pseudoscalar condensate, thus only the components $a = 0, 8$ of c_a are nonzero.

The pure gauge potential $V(L, L^*)$ for Polyakov loop $L \equiv \frac{1}{N_c} \text{Tr}_c e^{i g_s \int_0^{1/T} dx_4 \mathcal{A}^4}$ would take the form given by Munich group [29]:

$$\begin{aligned} \frac{V(L, L^*)}{T^4} &= -\frac{a \left(\frac{T}{T_0} \right)}{2} |L|^2 - \frac{0.75}{6} (L^3 + L^{*3}) + \frac{7.5}{4} |L|^4, \\ a(x) &= 6.75 - \frac{1.95}{x} + \frac{2.625}{x^2} - \frac{7.44}{x^3}, \end{aligned} \quad (3)$$

since it predicts a consistent temperature for chiral transition and deconfinement as from lattice QCD simulations [28]. Due to the interaction term $\sim \mathcal{A}^4$ between gluons and quarks, L would affect quark dynamics explicitly. In principle, quarks would also affect gluon dynamics. To account for the feedback, we simply modify T_0 according to the corrections of the two-loop β -function of QCD [30], that is,

$$T_0 = T_\tau e^{-\frac{1/\alpha_s}{b(N_f, \mu_B)}}, \quad b(N_f, \mu_B) = \frac{33 - 2N_f}{6\pi} - \frac{16N_f}{\pi} \left(\frac{\mu_B}{2T_\tau} \right)^2 \quad (4)$$

with $T_\tau = 1.77$ GeV, $\alpha_s = 0.304$ and $N_f = 3$.

B. The gap equations

By integrating over the quark degrees of freedom, the Lagrangian can be bosonized as

$$\begin{aligned} \mathcal{L}_{\text{PQM}} = & \text{Tr} \ln \left[i \not{\partial} - i \gamma^4 \left(i g_s \mathcal{A}^4 + Q_q \mu_Q + \frac{\mu_B}{3} \right) - g_m T^a \left(\sigma_a + i \gamma^5 \pi_a \right) \right] + \text{Tr} \left(\mathcal{D}_\mu^\dagger \phi^\dagger \mathcal{D}^\mu \phi - m_\phi^2 \phi^\dagger \phi \right) \\ & - h_1 [\text{Tr}(\phi^\dagger \phi)]^2 - h_2 \text{Tr}[(\phi^\dagger \phi)^2] + K [\text{Det}(\phi^\dagger) + \text{Det}(\phi)] + c_a \text{Tr} T^a (\phi^\dagger + \phi) - V(L, L^*). \end{aligned} \quad (5)$$

In energy momentum space, the Lagrangian becomes

$$\begin{aligned} \mathcal{L}_{\text{PQM}} = & \text{Tr} \ln \left[\not{k} - i\gamma^4 \left(ig_s \mathcal{A}^4 + Q_q \mu_Q + \frac{\mu_B}{3} \right) - g_m T^a \left(\sigma_a + i\gamma^5 \pi_a \right) \right] - \text{Tr} \left[(iq_4 - Q_m \mu_Q)^2 + \mathbf{k}^2 + m_\phi^2 \right] \phi^\dagger \phi \\ & - h_1 [\text{Tr}(\phi^\dagger \phi)]^2 - h_2 \text{Tr}[(\phi^\dagger \phi)^2] + K [\text{Det}(\phi^\dagger) + \text{Det}(\phi)] + c_a \text{Tr} T^a (\phi^\dagger + \phi) - V(L, L^*), \end{aligned} \quad (6)$$

where $\not{k} \equiv -\gamma^4 k_4 - \gamma \cdot \mathbf{k}$ and the summations over the internal energy momenta should be understood in the interaction terms. In heavy ion collisions, μ_Q is usually smaller than μ_B , so we only trivially expect chiral condensates (σ_0, σ_8) and Polyakov loop (L, L^*) to be nonzero in the ground state. For simplicity, their expectation values are assumed to be homogeneous over the space; then in mean field approximation, the thermodynamic potential can be derived as [28]

$$\begin{aligned} \Omega_{\text{PQM}} = & V(L, L^*) + m_\phi^2 (2\sigma_1^2 + \sigma_s^2) + h_1 (2\sigma_1^2 + \sigma_s^2)^2 + h_2 (2\sigma_1^4 + \sigma_s^4) - 2K\sigma_1^2 \sigma_s - 2c_1 \sigma_1 - c_s \sigma_s \\ & - 2T \sum_{f=u,d,s}^{t=\pm} \int_{-\infty}^{\infty} \frac{d^3 k}{(2\pi)^3} \ln \left[1 + 3L^{(t)} H_f^t + 3L^{(-t)} (H_f^t)^2 + (H_f^t)^3 \right], \quad H_f^t(E_{\mathbf{k}}^f, \mu_Q, \mu_B) \equiv e^{-\frac{1}{T}(E_{\mathbf{k}}^f - t(q_f \mu_Q + \frac{\mu_B}{3}))} \end{aligned} \quad (7)$$

where $L^{(+)} \equiv L, L^{(-)} \equiv L^*$ and $E_f = \sqrt{k^2 + m_f^2}$ with the dynamical masses $m_u = m_d = g_m \sigma_1$ and $m_s = g_m \sigma_s$. Note that it is more convenient to use the chiral condensates $\sigma_1 \equiv \frac{1}{2\sqrt{3}}(\sqrt{2}\sigma_0 + \sigma_8)$ and $\sigma_s \equiv \frac{1}{2\sqrt{3}}(\sqrt{2}\sigma_0 - 2\sigma_8)$ instead of σ_0 and σ_8 to present the thermodynamic potential, as they are directly related to quark masses. Another very important thing: By following the standard treatment [30], the divergent vacuum fluctuations of quarks are gotten rid of through renormalizations of the coupling constants in the mesonic sector. Without inducing confusions, we still keep the original denotations for the coupling constants, but keep in mind that they always refer to the renormalized ones in the following.

Usually, the Polyakov loop is taken to be real for simplicity, that is $L = L^*$, then the thermodynamic potential becomes

$$\begin{aligned} \Omega_{\text{PQM}} = & V(L, L) + m_\phi^2 (2\sigma_1^2 + \sigma_s^2) + h_1 (2\sigma_1^2 + \sigma_s^2)^2 + h_2 (2\sigma_1^4 + \sigma_s^4) - 2K\sigma_1^2 \sigma_s - 2c_1 \sigma_1 - c_s \sigma_s \\ & + 2T \sum_{f=u,d,s}^{t=\pm} \int_{-\infty}^{\infty} \frac{d^3 k}{(2\pi)^3} \ln F_f^t(E_{\mathbf{k}}^f, L, \mu_Q, \mu_B), \quad F_f^t(E_{\mathbf{k}}^f, L, \mu_Q, \mu_B) \equiv [1 + 3L H_f^t + 3L (H_f^t)^2 + (H_f^t)^3]^{-1}. \end{aligned} \quad (8)$$

And the gap equations follow the extremal conditions $\partial\Omega_{\text{PQM}}/\partial X = 0$, ($X = L, \sigma_1, \sigma_s$) as

$$\left[-a \left(\frac{T}{T_0} \right) L - 0.75L^2 + 7.5L^3 \right] T^4 - 6T \sum_{f=u,d,s}^{t=\pm} \int_{-\infty}^{\infty} \frac{d^3 k}{(2\pi)^3} [H_f^t + (H_f^t)^2] F_f^t = 0, \quad (9)$$

$$4m_\phi^2 \sigma_1 + 8h_1 (2\sigma_1^2 + \sigma_s^2) \sigma_1 + 8h_2 \sigma_1^3 - 4K\sigma_1 \sigma_s - 2c_1 + 6 \sum_{f=u,d}^{t=\pm} \int_{-\infty}^{\infty} \frac{d^3 k}{(2\pi)^3} \frac{g_m^2 \sigma_1}{E_{\mathbf{k}}^f} [L H_f^t + 2L (H_f^t)^2 + (H_f^t)^3] F_f^t = 0, \quad (10)$$

$$2m_\phi^2 \sigma_s + 4h_1 (2\sigma_1^2 + \sigma_s^2) \sigma_s + 4h_2 \sigma_s^3 - 2K\sigma_1^2 - c_s + 6 \sum_{f=s}^{t=\pm} \int_{-\infty}^{\infty} \frac{d^3 k}{(2\pi)^3} \frac{g_m^2 \sigma_s}{E_{\mathbf{k}}^s} [L H_s^t + 2L (H_s^t)^2 + (H_s^t)^3] F_s^t = 0. \quad (11)$$

For the case $\mu_Q = 0$, it is easy to check that Eqs. (10) and (11) imply $\sigma_1 = \sigma_s$ in the limit $c_1 = c_s$, that is, when s quark is degenerate with the light quarks. Moreover, in the chiral limit $c_1 = 0$, we find a trivial solution $\sigma_1 = 0$ to Eqs. (10) thus exact chiral symmetry is realized for the light quarks and mesons in the Lagrangian.

C. The static and pole energies of mesons

Now we are going to explore mesonic spectra by taking Taylor expansions over mesonic fluctuations in Eq.(5) based on the mean field values of σ_1, σ_s and L . Keep quadratic terms for a few lightest mesons that we are interested in,

that is, σ , π , and K mesons, we have

$$\begin{aligned} \mathcal{L}_{\text{PQM}}^2 &= -\frac{1}{2V_4} \text{Tr} \left[G(x, x') g_m T^a \left(\hat{\sigma}_a(x') + i\gamma^5 \hat{\pi}_a(x') \right) G(x', x) g_m T^{a'} \left(\hat{\sigma}_{a'}(x) + i\gamma^5 \hat{\pi}_{a'}(x) \right) \right] - \frac{1}{2} \hat{\sigma} (\partial_\mu \partial^\mu + m_\phi^2) \hat{\sigma} \\ &\quad - \frac{1}{2} \hat{\pi}^0 (\partial_\mu \partial^\mu + m_\phi^2) \hat{\pi}^0 - \hat{\pi}^- (\mathcal{D}_\mu \mathcal{D}^\mu + m_\phi^2) \hat{\pi}^+ - \hat{K}^{0*} (\partial_\mu \partial^\mu + m_\phi^2) \hat{K}^0 - \hat{K}^- (\mathcal{D}_\mu \mathcal{D}^\mu + m_\phi^2) \hat{K}^+ \\ &\quad - h_1 \left[(6\sigma_1^2 + \sigma_s^2) \hat{\sigma}^2 + (2\sigma_1^2 + \sigma_s^2) (2\hat{\pi}^+ \hat{\pi}^- + (\hat{\pi}^0)^2) + 2\hat{K}^+ \hat{K}^- + 2\hat{K}^{0*} \hat{K}^0 \right] - h_2 \left[3\sigma_1^2 \hat{\sigma}^2 + \sigma_1^2 (2\hat{\pi}^+ \hat{\pi}^- + (\hat{\pi}^0)^2) \right. \\ &\quad \left. + 2(\sigma_s^2 + \sigma_1^2 - \sigma_1 \sigma_s) (\hat{K}^+ \hat{K}^- + \hat{K}^{0*} \hat{K}^0) \right] + \kappa \left[\frac{\sigma_s}{2} \hat{\sigma}^2 + \sigma_s \left(\hat{\pi}^+ \hat{\pi}^- + \frac{1}{2} (\hat{\pi}^0)^2 \right) + \sigma_1 (\hat{K}^+ \hat{K}^- + \hat{K}^{0*} \hat{K}^0) \right] \quad (12) \end{aligned}$$

with $\hat{\sigma}$ the fluctuation of σ_1 and the full quark propagator

$$\begin{aligned} G(x, x') &\equiv \text{diag}(G_u(x, x'), G_d(x, x'), G_s(x, x')) \\ &= i [i\hat{\phi} - i\gamma^4 \left(ig_s \mathcal{A}^4 + Q_q \mu_Q + \frac{\mu_B}{3} \right) - g_m T^a \sigma_a]^{-1} \quad (13) \end{aligned}$$

Usually, the expectation value of \mathcal{A}^4 is taken to be a diagonal and traceless constant matrix in color space, that is, $g_s \mathcal{A}^4 = T \text{diag}(p_1, p_2, p_3)$ with $p_1 + p_2 + p_3 = 0$. Then, the quark propagators in flavor and color spaces are, respectively,

$$G_{f,c}(x, x') = i [i\hat{\phi} - i\gamma^4 \left(ip_c T + Q_f \mu_Q + \frac{\mu_B}{3} \right) - g_m \sigma_f]^{-1} \quad (14)$$

with $f = u, d, s; c = 1, 2, 3$, and become

$$G_{f,c}(k) = i [-\not{k} - i\gamma^4 \left(ip_c T + Q_f \mu_Q + \frac{\mu_B}{3} \right) - g_m \sigma_f]^{-1} \quad (15)$$

in energy momentum space. Actually, it is by applying (15) that the expression (7) is derived.

Since the full quark propagator $G(x, x')$ is diagonal in flavor and color spaces, only the ones with $T^{a\dagger} = T^{a'}$ are nonzero for the first term in (12). Then, for σ , π and K mesons, the corresponding polarization functions should be evaluated according to

$$\Pi_{\hat{\sigma}} = -\frac{g_m^2}{8V_4} \sum_{f=u,d}^{c=r,g,b} \text{tr}[G_{f,c}(k+q) G_{f,c}(k)], \quad (16)$$

$$\Pi_{\hat{\pi}^0} = -\frac{g_m^2}{8V_4} \sum_{f=u,d}^{c=r,g,b} \text{tr}[G_{f,c}(k+q) i\gamma^5 G_{f,c}(k) i\gamma^5], \quad (17)$$

$$\Pi_{\hat{\pi}^+} = -\frac{g_m^2}{2V_4} \sum_{f=u,d}^{c=r,g,b} \text{tr}[G_{u,c}(k+q) i\gamma^5 G_{d,c}(k) i\gamma^5], \quad (18)$$

$$\Pi_{\hat{K}^0} = -\frac{g_m^2}{2V_4} \sum_{f=u,d}^{c=r,g,b} \text{tr}[G_{s,c}(k+q) i\gamma^5 G_{d,c}(k) i\gamma^5], \quad (19)$$

$$\Pi_{\hat{K}^+} = -\frac{g_m^2}{2V_4} \sum_{f=u,d}^{c=r,g,b} \text{tr}[G_{u,c}(k+q) i\gamma^5 G_{s,c}(k) i\gamma^5], \quad (20)$$

where the traces tr are only over Dirac matrices and energy momentum space. The explicit evaluations and renormalizations are given in Appendix. A. There are usually energy momentum independent and dependent

terms in the vacuum parts of the polarization functions: The independent terms are simultaneously gotten rid of by the renormalizations of the coupling constants in the mesonic sector, but the dependent terms is not relevant to that thus should be kept, see (A2) for example. Actually, the latter is essential to unlock the moat boundaries from the transition line of chiral symmetry, see the discussions at the end of Appendix. B. If the latter is not properly renormalized but regularized by an energy momentum cutoff Λ , such as done in Nambu–Jona-Lasino model, the quark loops always contribute positively to the wave function renormalizations within the effective range $T, \mu_B < \Lambda$, thus no moat regimes can be justified at all.

Eventually, the mesonic propagators, generally denoted by $G_m(iq_4 - q_m \mu_Q, \mathbf{q})$ ($m = \hat{\sigma}, \hat{\pi}^0, \hat{\pi}^+, \hat{K}^0, \hat{K}^+$), can be obtained as

$$G_{\hat{\sigma}}^{-1}(iq_4, \mathbf{q}) = q_4^2 + \mathbf{q}^2 + \tilde{m}_{\hat{\sigma}}^2 + 2\Pi_{\hat{\sigma}}(iq_4, \mathbf{q}), \quad (21)$$

$$G_{\hat{\pi}^0}^{-1}(iq_4, \mathbf{q}) = q_4^2 + \mathbf{q}^2 + \tilde{m}_{\hat{\pi}^0}^2 + 2\Pi_{\hat{\pi}^0}(iq_4, \mathbf{q}), \quad (22)$$

$$G_{\hat{\pi}^+}^{-1}(iq_4, \mathbf{q}) = Q_4^2 + \mathbf{q}^2 + \tilde{m}_{\hat{\pi}^+}^2 + \Pi_{\hat{\pi}^+}(iq_4, \mathbf{q}), \quad (23)$$

$$G_{\hat{K}^0}^{-1}(iq_4, \mathbf{q}) = q_4^2 + \mathbf{q}^2 + \tilde{m}_{\hat{K}^0}^2 + \Pi_{\hat{K}^0}(iq_4, \mathbf{q}), \quad (24)$$

$$G_{\hat{K}^+}^{-1}(iq_4, \mathbf{q}) = Q_4^2 + \mathbf{q}^2 + \tilde{m}_{\hat{K}^+}^2 + \Pi_{\hat{K}^+}(iq_4, \mathbf{q}) \quad (25)$$

with $iQ_4 \equiv iq_4 - e\mu_Q$ and the tree-level effective masses:

$$\tilde{m}_{\hat{\sigma}}^2 \equiv m_\phi^2 + 2h_1(6\sigma_1^2 + \sigma_s^2) + 6h_2\sigma_1^2 - \kappa\sigma_s, \quad (26)$$

$$\tilde{m}_{\hat{\pi}^0}^2 \equiv m_\phi^2 + 2h_1(2\sigma_1^2 + \sigma_s^2) + 2h_2\sigma_1^2 - \kappa\sigma_s, \quad (27)$$

$$\tilde{m}_{\hat{K}^0}^2 \equiv m_\phi^2 + 2h_1(2\sigma_1^2 + \sigma_s^2) + 2h_2(\sigma_s^2 + \sigma_1^2 - \sigma_1\sigma_s) - \kappa\sigma_1. \quad (28)$$

One note that $G_m(iq_4 - q_m \mu_Q, \mathbf{q})$ does not depend on the direction of \mathbf{q} as the system is isotropic, so we can simply consider $G_m(iq_4 - q_m \mu_Q, |\mathbf{q}|)$ instead. For $\mu_Q = 0$, we can easily see that $\hat{\pi}^0$ is degenerate with $\hat{\pi}^\pm$ by comparing (22) and (23), and \hat{K}^0 is degenerate with \hat{K}^\pm by comparing (24) and (25). However, kaons are not necessarily degenerate with their antiparticles at finite μ_B due to the mass and thus density splitting between s and light quarks.

To study the moat regimes, the static energies, defined by $E_m(|\mathbf{q}|) \equiv G_m^{-1/2}(0, |\mathbf{q}|)$ in the limit $\mu_Q = 0$, are relevant, and the boundaries are determined by the sign

change of the wave function renormalizations,

$$Z_m^\perp \equiv \frac{1}{2} \frac{\partial^2 E_m^2}{\partial |\mathbf{q}|^2} \Big|_{|\mathbf{q}|=0}, \quad (29)$$

see the derivations in Appendix. B. On the other hand, to study the dynamical effects of mesons, the pole energies are more relevant and could be evaluated self-consistently by requiring $G_m^{-1}(-q_0(|\mathbf{q}|), |\mathbf{q}|) = 0$ for a given $|\mathbf{q}|$. According to the FRG-QCD calculations [26], the static energies would show minima at finite $|\mathbf{q}|$ when both T and μ_B are large, but the pole energies are always the smallest at $|\mathbf{q}| = 0$. Such a feature would be checked in a much wider region in this work. Before that, we would like to point out that there is a universal and consistent expression for the static and pole energies when the momentum $|\mathbf{q}|$ is large, that is, $E_m \approx q_0(|\mathbf{q}|) \approx |\mathbf{q}|$. It is because the leading contributions of the polarization functions are $\sim \ln |\mathbf{q}|^2$ for the static case and $|\mathbf{q}|$ -independent for $q_0^2 = |\mathbf{q}|^2 + m_m^2$, see the discussions at the end of Appendix. A.

III. NUMERICAL CALCULATIONS AND DISCUSSIONS

In the following, we will take $\mu_Q = 0$ and focus on the $T - \mu_B$ plane. To perform numerical calculations, the model parameters should be fixed first. As the quark-gluon coupling constant g_s could eventually be absorbed into the definition of the Polyakov loop which is then determined according to the gap equations, there are seven unknown model parameters in the quark-meson sector. The coupling constants h_2, κ, c_0 and c_8 can be fixed as [31]

$$\begin{aligned} h_2 &= 46.5, \kappa = 4810 \text{ MeV}, c_0 = (286 \text{ MeV})^3, \\ c_8 &= -(311 \text{ MeV})^3 \end{aligned} \quad (30)$$

by utilizing the well determined experimental results for pion decay constant and pseudoscalar meson masses in the vacuum,

$$\begin{aligned} f_\pi &= 92.4 \text{ MeV}, m_\pi = 138 \text{ MeV}, m_K = 496 \text{ MeV}, \\ m_{\eta'} &= 963 \text{ MeV}, m_\eta = 539 \text{ MeV}. \end{aligned} \quad (31)$$

The corresponding coupling constants in the linear terms of σ_1 and σ_s are $c_1 = (121 \text{ MeV})^3$ and $c_s = (378 \text{ MeV})^3$, respectively.

However, there are quite large biases in the scalar meson masses: According to the Particle Group Data, the T-matrix pole mass of the lowest energy eigenstate $f(500)$ lies in the range $400 \sim 550$ MeV. So we will take the average mass $m_{f(500)} = 475$ MeV as the center value to fix the parameter g_m by fitting to the first-principle results, and then the parameters m_ϕ and h_1 change correspondingly with the value of $m_{f(500)}$ for the given pseudoscalar masses. Note that $f(500)$ is a mixed state of $\hat{\sigma}$ and $\hat{\sigma}_s$ due to chiral anomaly [31]. According to recent

lattice QCD simulations, the pseudo-critical temperature at zero baryon density is $T_c = 156 \pm 1.5$ MeV [7]; and the FRG-QCD calculations predicted the critical end point to be at $(T_{\text{CEP}}, \mu_{\text{B(CEP)}}) = (107, 635)$ MeV [12]. Fitting to $T_c = 156$ MeV and $\mu_{\text{B(CEP)}} = 635$ MeV, the quark-meson coupling constant can be fixed to $g_m = 5.756$. And the values of m_ϕ and h_1 are listed in Table.I with respect to $m_{f(500)}$.

TABLE I. The model parameters m_ϕ and h_1 .

| $m_{f(500)}$ (MeV) | m_ϕ (MeV) | h_1 |
|--------------------|----------------|--------|
| 400 | 495 | -5.90 |
| 475 | 452 | -3.58 |
| 550 | 394 | -0.776 |

A. The $T - \mu_B$ phase diagram

As has mentioned, we take the center value of $f(500)$ mass to be 475 MeV, then $m_{f(500)} = 400, 550$ MeV can be used to estimate error bars. For the parameters given in Table.I, the $T - \mu_B$ phase diagram can be obtained by solving the gap equations and comparing the thermodynamic potentials between different solutions. The results are illustrated in Fig. 1 for chiral transition of light quarks and deconfinement together with other theoretical predictions of CEP. Note that for crossover, the

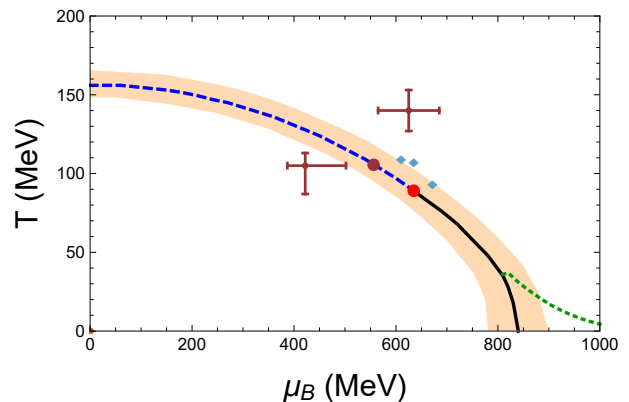


FIG. 1. The $T - \mu_B$ phase diagram in the Polyakov-Quark-Meson model with the blue dashed line crossover, the black solid line first-order chiral transition and the red bullet the critical end point at (635, 89) MeV. The green dotted line indicates the deconfinement crossover that starts to split from the first-order chiral transition at large μ_B . Other theoretical predictions of CEP are also shown for comparison: the cyan diamonds are from functional renormalization approaches [12–14], and the biased deep-red points are from left to right given by lattice QCD simulations with complex baryon chemical potential [16], holographic QCD [15], and finite-size scaling analysis [17], respectively.

pseudocritical temperatures are determined by the quickest change points of the order parameters. In the PQM model, the (pseudo-)critical temperature of chiral transition is consistent with that of deconfinement up to large μ_B , thus agrees with those found for crossover in lattice QCD simulations [6, 7]. As we can see from Fig. 1, the transition region is quite consistent the CEPs from functional renormalization approaches [12–14] and holographic QCD [15], but lies between the CEPs from lattice QCD simulations with complex baryon chemical potential [16] and finite-size scaling analysis [17].

Well before the critical baryon chemical potential of chiral transition at zero temperature, $\mu_B^c \sim 850$ MeV, an extra peak begins to show up in the slope of L with respect to T , implying splitting between chiral transition and deconfinement. So, there is a region where chiral symmetry is restored but confinement remains at large μ_B and small T — the so-called "quarkyonic matter" phase. One might notice that the μ_B^c found here is even smaller than that of gas-liquid transition of symmetric nuclear matter, it is because the nucleon degrees of freedom are not efficiently taken into account in the PQM model and the supposed gas-liquid transition is missing. Finally, to demonstrate the occurrence of phase transition explicitly, we show the order parameters, light quark mass m_1 and Polyakov loop L , as functions of temperature for different baryon chemical potentials in Fig. 2

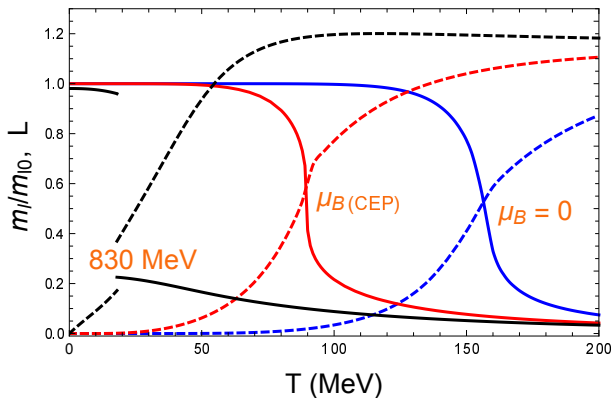


FIG. 2. The order parameters, light quark mass m_1 (reduced by its vacuum value m_{10}) and Polyakov loop L as functions of temperature T for three baryon chemical potentials: 0, $\mu_{B(\text{CEP})}$ and 830 MeV.

B. The moat regimes

The moat regimes for σ, π and K^+ mesons are illustrated together with the phase boundaries in Fig. 3. As we can see, the moat regime for K^+ meson occurs at larger T and μ_B than those for σ and π , but the main features are the same. So we will focus on the moat regimes for σ and π in the following.

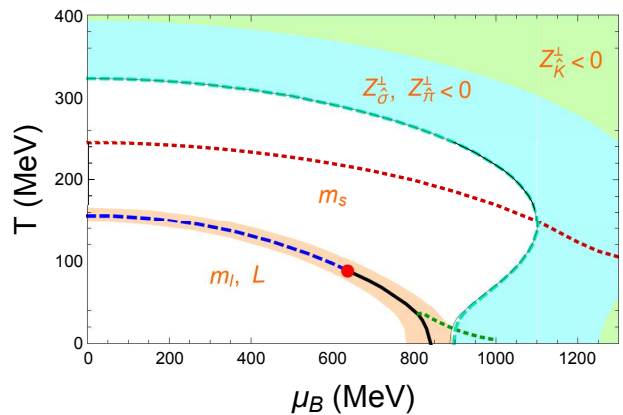


FIG. 3. The moat regimes presented by $Z_\sigma^\perp, Z_\pi^\perp$ and $Z_K^\perp < 0$ for σ, π and K^+ mesons in the PQM model: cyan for σ and π , and light green for K^+ . The cyan dashed line and thin black line are the corresponding moat boundaries of σ and π , respectively, and the purple dashed and solid lines are those from FRG-QCD calculations. The phase boundaries are also shown with the denotations following Fig. 1 and the extra deep-red dotted line for the crossover of s-quark.

Consistent with previous findings [26, 27], the moat regimes for the chiral partners σ and π are always in the chiral symmetry restoration phase of light quarks, and due to that they closely overlap with each other. However, at the lower temperature end, it is slightly visible that the moat boundaries of π and σ split from each other with that of π wider. In the following, we try to understand that feature by analyzing the wave function renormalizations given in Eqs. (B23) and (B24) in the zero temperature limit.

If we look at their vacuum parts, Z_σ^\perp should be smaller than Z_π^\perp by $\frac{g_m^2}{8\pi^2} \left(1 - \frac{m_1^2}{m_\sigma^2}\right)$, so the inversion of their actual relative values must come from the thermal part proportional to m_1^2 in Z_σ^\perp . At zero temperature, the system is fully confined with $L = 0$, hence $Q_f^{-(2)} = 0$ in Z_σ^\perp and $Q_f^{+(2)}$ can be evaluated explicitly as

$$\begin{aligned} Q_f^{+(2)} &\approx - \int_0^\infty \frac{dk}{24\pi^2 k^2} \left[\frac{1}{E_{\mathbf{k}}^f} \theta\left(\frac{\mu_B}{3} - E_{\mathbf{k}}^f\right) - \frac{1}{m_f} \right] \\ &= - \int_0^{k_F} \frac{dk}{24\pi^2 k^2} \left[\frac{1}{E_{\mathbf{k}}^f} - \frac{1}{m_f} \right] + \frac{1}{24\pi^2 m_f k_F} \\ &= \frac{\mu_B}{72\pi^2 m_f^2 k_F} \end{aligned} \quad (32)$$

with $\theta(x)$ the step function and $k_F \equiv \sqrt{\left(\frac{\mu_B}{3}\right)^2 - m_f^2}$ the Fermi momentum. Beyond μ_B^c , $m_f \ll \frac{\mu_B}{3}, m_{10}$, thus the

difference between Z_{σ}^{\perp} and Z_{π}^{\perp} can be evaluated as

$$\begin{aligned} Z_{\sigma}^{\perp} - Z_{\pi}^{\perp} &= \frac{g_m^2}{8\pi^2} \left(\frac{\mu_B}{3k_F} - 1 + \frac{m_1^2}{m_{10}^2} \right) \\ &\approx \frac{g_m^2}{8\pi^2} \left(\frac{m_1^2}{2\left(\frac{\mu_B}{3}\right)^2} + \frac{m_1^2}{m_{10}^2} \right) > 0. \end{aligned} \quad (33)$$

With respect to that, it is easy to understand why the moat regime of π should cover that of σ when increasing temperature for a given μ_B . In chiral limit, $m_1 = 0$ in the chiral symmetry restoration phase, and the moat boundaries of σ and π would exactly overlap with each other.

Moreover, with decreasing temperature, we find that the moat boundaries of π and σ bend back to baryon chemical potentials well beyond μ_B^c at zero temperature and are far away from the chiral transition line except the lower temperature end. All the features are qualitatively consistent with those found in QM model [27], and the former feature actually implies reentrance of moat regimes well beyond μ_B^c . As has mentioned, the moat boundaries are consistent with the CEP and chiral crossover line therefrom up to around $T = 140$ MeV in FRG-QCD calculations [26], see the purple lines in Fig. 3. Hence, including the effects of strange quark and confinement in the 2+1 flavor PQM model cannot help to bridge the gap between the predictions of QM model and FRG-QCD. The reentrance of moat regimes is of course due to the interplay between T and larger μ_B , in the following we try to understand that by focusing on $Q_f^{t(0)}$ in the wave function renormalization Z_{π}^{\perp} .

For most of the reentrance region, the moat boundaries are on top of the deconfinement line, see the green dashed line in Fig. 3, so we will take $L = 1$ for simplicity and then $Q_f^{t(0)}$ is reduced to

$$Q_f^{t(0)} = - \int_0^{\infty} \frac{dk}{2\pi^2} \frac{1}{E_{\mathbf{k}}^f} \frac{1}{1 + e^{\frac{1}{T}(E_{\mathbf{k}}^f - t\frac{\mu_B}{3})}} \quad (34)$$

with $m_f \ll \frac{\mu_B}{3}$. As we have pointed out in Appendix. B, the whole thermal part $\sum_{t=\pm} Q_f^{t(0)}$ gives rise to a term $\sim \ln m_f$ that exactly cancels the one from vacuum polarization in the limit $m_f \rightarrow 0$. To discuss the variation of the thermal part with T for a given μ_B , we take the derivative with respect to T and have

$$\frac{\partial \bar{Q}_f^{(0)}}{\partial T} = - \frac{1}{T^2} \int_0^{\infty} \frac{dk}{2\pi^2} \sum_{t=\pm} \frac{(E_{\mathbf{k}}^f - t\frac{\mu_B}{3}) e^{\frac{1}{T}(E_{\mathbf{k}}^f - t\frac{\mu_B}{3})}}{E_{\mathbf{k}}^f \left(1 + e^{\frac{1}{T}(E_{\mathbf{k}}^f - t\frac{\mu_B}{3})}\right)^2}. \quad (35)$$

This is convergent in the limit $m_f \rightarrow 0$, so we consider such a limit for simplicity and get

$$\frac{\partial \bar{Q}_f^{(0)}}{\partial T} = \frac{H(\tilde{\mu}_B)}{T}, \quad H(\tilde{\mu}_B) \equiv - \int_0^{\infty} \frac{d\tilde{k}}{2\pi^2} \frac{1}{\tilde{k}} \sum_{t=\pm} \frac{(\tilde{k} - t\frac{\tilde{\mu}_B}{3}) e^{\tilde{k} - t\frac{\tilde{\mu}_B}{3}}}{\left(1 + e^{\tilde{k} - t\frac{\tilde{\mu}_B}{3}}\right)^2} \quad (36)$$

with $\tilde{k} \equiv k/T$ and $\tilde{\mu}_B \equiv \mu_B/T$.

The sign of $H(\tilde{\mu}_B)$ controls the monotonic behavior of $\bar{Q}_f^{(0)}$ with respect to T : increasing for $H(\tilde{\mu}_B) > 0$ and decreasing for $H(\tilde{\mu}_B) < 0$. As shown in Fig. 4, the sign of $H(\tilde{\mu}_B)$ changes around $\tilde{\mu}_B = 7$. So start from the moat

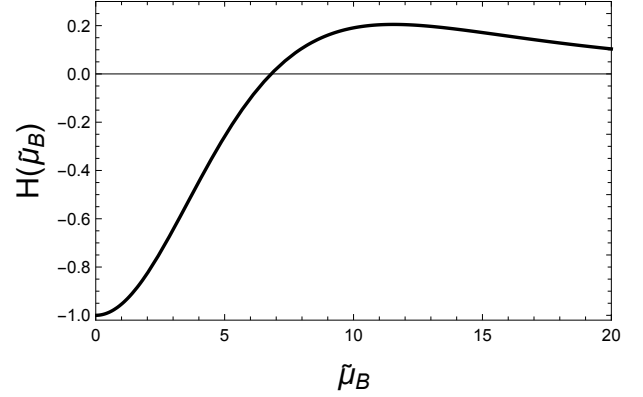


FIG. 4. The auxiliary function $H(\tilde{\mu}_B)$ with $\tilde{\mu}_B \equiv \mu_B/T$.

regime for a large μ_B at zero temperature, $\bar{Q}_f^{(0)}$ increases with T firstly and then decreases, indicating a peak in Z_{π}^{\perp} . In the PQM model, the peak of Z_{π}^{\perp} is positive well beyond μ_B^c thus reentrance is found; for even larger μ_B , the peak is negative and the whole temperature region is in moat regime. In a word, the reentrance happens because temperature favors moat regime itself on one hand but reduces the chemical potential effect through $\tilde{\mu}_B$ on the other hand. For comparison, the baryon number density from light quarks takes the form

$$n_B \approx \int_0^{\infty} \frac{k^2 dk}{\pi^2} \sum_{t=\pm} \frac{t}{1 + e^{\frac{1}{T}(k - t\frac{\mu_B}{3})}} = \frac{\mu_B}{9} \left[T^2 + \left(\frac{\mu_B}{3\pi}\right)^2 \right] \quad (37)$$

in the chiral symmetry restoration phase, monotonically increasing with T for a given μ_B . Actually, the main difference between (34) and (37) is the order of k in the integrand, and temperature does not suppress chemical potential effect at all in Eq. (37).

We demonstrate the full calculations of Z_{π}^{\perp} in Fig. 5 where the effects of chiral symmetry breaking and restoration and (de-)confinement are taken into account self-consistently. As can be seen, there are always local peaks in the curves for all μ_B except $\mu_{B(\text{CEP})}$, but the reasons are quite different. For $\mu_B < \mu_{B(\text{CEP})}$, the peaks and dips are caused by the chiral crossover with their locations consistent with the pseudo-critical temperatures and eventually merging into a point of reflection at $\mu_{B(\text{CEP})}$. For $\mu_B > \mu_{B(\text{CEP})}$, the peaks separate from the chiral transition points and are due to the non-monotonic feature of $\bar{Q}_f^{(0)}$ in the chiral symmetry restoration phase, as has just been discussed. For a small μ_B , we can only find one zero point for Z_{π}^{\perp} because it is shifted to a larger value due to chiral symmetry breaking at the

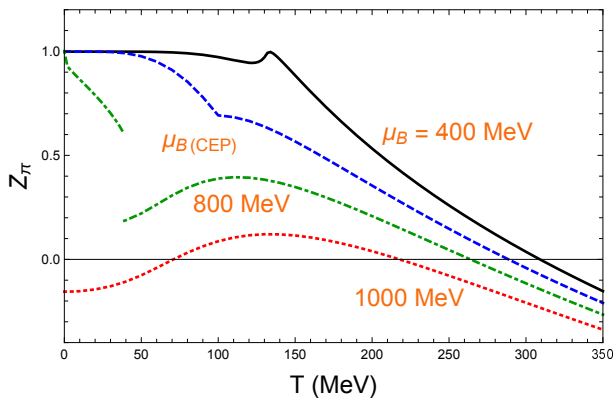


FIG. 5. The wave function renormalization of π mesons, Z_{π}^{\perp} , as a function of temperature T for different baryon chemical potentials, $\mu_B = 400, 635$ ($\mu_{B(\text{CEP})}$), 800 and 1000 MeV.

lower temperature end. The latter can be understood more physically: The pseudo-Goldstone bosons, pions, dominate the thermodynamics in the chiral symmetry breaking phase. If $Z_{\pi}^{\perp} < 0$ there, the sound velocity square would be negative, which means that the pressure unphysically decreases with the energy for a pion gas. For a μ_B well beyond μ_B^c , there are two zero points that can account for the reentrance feature of Z_{π}^{\perp} .

In that sense, the moat boundaries of π and σ mesons found in FRG-QCD calculations [26] can be understood in the following way. The lower branches, consistent with chiral crossover line, are of course caused by chiral symmetry restoration where the dips are more significant than ours. And the upper branches correspond to the lower branches of the reentrance region found in our work, where the temperature increases with μ_B . If the calculations are extended to larger temperature in FRG-QCD, we are supposed to find the top branches of the reentrance region where the temperature decreases with μ_B . It was pointed out in Ref. [26] that the moat regimes are mainly dominated by particle-particle contributions (or Landau damping), such an observation can be easily justified by look at the pole structure $1/\mathbf{q} \cdot \mathbf{k}$ in the integrand of (B2). For particle-antiparticle contributions, the structure $(E_{\mathbf{k}+\mathbf{q}/2}^f + E_{\mathbf{k}-\mathbf{q}/2}^f)^{-1}$ is involved and no pole is found in the limit $|\mathbf{q}| \rightarrow 0$; while for particle-particle contributions, the structure $(E_{\mathbf{k}+\mathbf{q}/2}^f - E_{\mathbf{k}-\mathbf{q}/2}^f)^{-1}$ is involved and the pole structure is recovered in the limit $|\mathbf{q}| \rightarrow 0$.

Finally, we present the pole energy $q_0(|\mathbf{q}|)$ of π as a function of momentum $|\mathbf{q}|$ in Fig. 6 for different values of temperature and baryon chemical potential. Consistent with FRG-QCD calculations [26], $q_0(|\mathbf{q}|)$ is always a monotonically increasing function of $|\mathbf{q}|$ regardless in the case of vacuum, high density or deep moat regime. Such a feature is also true for σ and K mesons, so the pole energy is rather different from the static energy, which could decrease with $|\mathbf{q}|$ when the wave function renor-

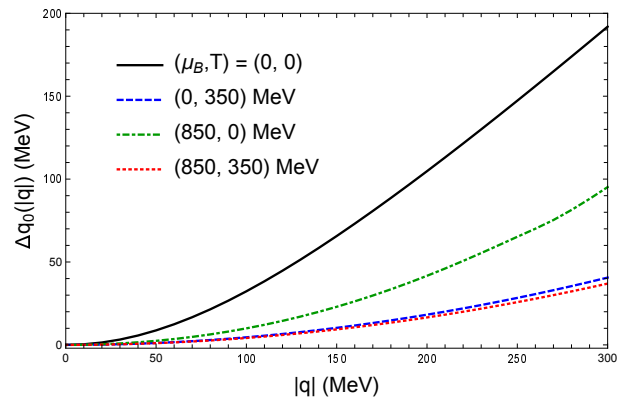


FIG. 6. The pole energy $q_0(|\mathbf{q}|)$ of π as a function of momentum $|\mathbf{q}|$ for different values of temperature and baryon chemical potential.

malization Z_m^{\perp} is negative. Since they are the same at the tree level, the difference must come from the quark loops and the wave function renormalization depends on the energy q_0 remarkably. Therefore, to explore dynamical properties in the medium, one should be careful not to take static energy to replace pole energy in the calculations.

IV. SUMMARY

In this work, the moat regime of QCD matter is explored within the realistic 2 + 1 flavor Polyakov-Quark-Meson model. Compared to the two-flavor Quark-Meson model, two more effects are further taken into account: strange quark and confinement coded through Polyakov loop. With proper model parameters, the $T - \mu_B$ phase diagram obtained is consistent with most predictions on the critical end point. And it is found that the basic features of moat regimes for σ and π mesons remain similar to those from Quark-Meson model: They cover the region where temperature or baryon chemical potential is large enough and are basically far away from the chiral transition line; reentrance occurs around the critical baryon chemical potential of chiral transition at zero temperature due to the competition between catalysis and chemical potential suppression effects of temperature. Hence, the effects of strange quark and confinement still cannot help to bridge the gap between the predictions of QM model and FRG-QCD.

Nevertheless, some basic features of the moat regimes found in FRG-QCD calculations can be understood qualitatively:

1. σ and π mesons are chiral partners, so their moat boundaries are close to each other in the chiral symmetry restoration phase.
2. Since chiral symmetry is not exact in QCD, the terms proportional to quark mass square would enhance the wave function renormalization of σ meson at larger tem-

perature or baryon chemical potential, hence its moat boundary lies well within that of pions.

3. The lower branches are caused by chiral symmetry restoration, the upper branches correspond to the lower branches of the reentrance region, and an extra top branches of the reentrance region are expected to exist.

The pole energy is also explored: Consistent with FRG-QCD calculations, it monotonically increases with momentum regardless in the case of vacuum, high density or deep moat regime. Finally, we would like to mention that the moat regime and pole energy of K mesons are also explored and they follow similar features to those of

σ and π mesons.

ACKNOWLEDGEMENT

G.C. thanks W.J. Fu from Dalian University of Technology and X.F. Luo from Central China Normal University for helpful discussions. The work is funded by the "Forefront Leading Project of Theoretical Physics" from the National Natural Science Foundation of China with Grant No. 12447102. G.C. is also supported by the Natural Science Foundation of Guangdong Province with Grant No. 2024A1515011225.

Appendix A: Evaluations of polarization functions

We take $\Pi_{\tilde{\sigma}}$ for example, it can be evaluated as the following:

$$\begin{aligned}
\Pi_{\tilde{\sigma}}(iq_4, \mathbf{q}) &= -\frac{g_m^2}{8} T \sum_n \sum_{f=u,d}^{c=r,g,b} \int \frac{d^3\mathbf{k}}{(2\pi)^3} \text{tr} \left[\frac{i}{-\not{k} - \not{q} - i\gamma^4(iq_c T + Q_f \mu_Q + \frac{\mu_B}{3}) - g_m \sigma_f} \frac{i}{-\not{k} - i\gamma^4(iq_c T + Q_f \mu_Q + \frac{\mu_B}{3}) - g_m \sigma_f} \right] \\
&= -\frac{g_m^2}{2} T \sum_n \sum_{f=u,d}^{c=r,g,b} \int \frac{d^3\mathbf{k}}{(2\pi)^3} \frac{(-(\omega_n + q_4) + q_c T - iQ_f \mu_Q - i\frac{\mu_B}{3})(-\omega_n + q_c T - iQ_f \mu_Q - i\frac{\mu_B}{3}) + (\mathbf{k} + \mathbf{q}) \cdot \mathbf{k} - m_f^2}{[(-(\omega_n + q_4) + q_c T - iQ_f \mu_Q - i\frac{\mu_B}{3})^2 + (\mathbf{k} + \mathbf{q})^2 + m_f^2][(-\omega_n + q_c T - iQ_f \mu_Q - i\frac{\mu_B}{3})^2 + \mathbf{k}^2 + m_f^2]} \\
&= \Pi_{\tilde{\sigma}}^Y - \frac{g_m^2}{4} \sum_{f=u,d}^{c=r,g,b} \int \frac{d^3\mathbf{k}}{(2\pi)^3} \sum_{u,t=\pm} \frac{-E_{\mathbf{k}+u\mathbf{q}/2}^f (E_{\mathbf{k}+u\mathbf{q}/2}^f + u t i q_4) + \mathbf{k}^2 - \mathbf{q}^2/4 - m_f^2}{E_{\mathbf{k}+u\mathbf{q}/2}^f [(E_{\mathbf{k}+u\mathbf{q}/2}^f + u t i q_4)^2 - (\mathbf{k} - u \mathbf{q}/2)^2 - m_f^2]} \frac{1}{1 + e^{[E_{\mathbf{k}+u\mathbf{q}/2}^f - t(iq_c T + Q_f \mu_Q + \frac{\mu_B}{3})]/T}} \\
&= \Pi_{\tilde{\sigma}}^Y - \frac{3g_m^2}{4} \sum_{f=u,d} \int \frac{d^3\mathbf{k}}{(2\pi)^3} \sum_{u,t=\pm} \frac{-u t E_{\mathbf{k}+u\mathbf{q}/2}^f (i q_4) - u \mathbf{q} \cdot \mathbf{k} - \mathbf{q}^2/2 - 2m_f^2}{E_{\mathbf{k}+u\mathbf{q}/2}^f [2u t E_{\mathbf{k}+u\mathbf{q}/2}^f (i q_4) + 2u \mathbf{q} \cdot \mathbf{k} + (i q_4)^2]} [L H_f^{ut} + 2L(H_f^{ut})^2 + (H_f^{ut})^3] F_f^{ut}, \quad (\text{A1})
\end{aligned}$$

where $H_f^{ut} \equiv H_f^t(E_{\mathbf{k}+u\mathbf{q}/2}^f; \mu_Q, \mu_B)$ and the vacuum term is renormalized in the following way:

$$\begin{aligned}
\Pi_{\tilde{\sigma}}^Y(q^2) &\equiv -\frac{3g_m^2}{2} \sum_{f=u,d} \int \frac{d^4k}{(2\pi)^4} \frac{-k \cdot (k+q) - m_f^2}{[-k^2 + m_f^2][-(k+q)^2 + m_f^2]} \\
&= -\frac{3g_m^2}{2} \sum_{f=u,d} \int \frac{d^4k}{(2\pi)^4} \frac{1}{-k^2 + m_f^2} - \frac{3g_m^2}{4} \sum_{f=u,d} \int \frac{d^4k}{(2\pi)^4} \frac{q^2 - 4m_f^2}{[-k^2 + m_f^2][-(k+q)^2 + m_f^2]} \\
&\Rightarrow -\frac{3g_m^2}{4} \sum_{f=u,d} \int \frac{d^4k}{(2\pi)^4} \frac{q^2 - 4m_f^2}{[-k^2 + m_f^2][-(k+q)^2 + m_f^2]} \\
&= \frac{3g_m^2}{2(4\pi)^2} \sum_{f=u,d} (q^2 - 4m_f^2) \left(\ln \frac{m_f}{m_{f0}} + \sqrt{1 - 4\frac{m_f^2}{q^2}} \text{arccoth} \sqrt{1 - 4\frac{m_f^2}{q^2}} - \sqrt{1 - 4\frac{m_{f0}^2}{q^2}} \text{arccoth} \sqrt{1 - 4\frac{m_{f0}^2}{q^2}} \right) \quad (\text{A2})
\end{aligned}$$

with m_{f0} ($f = u, d, s$) the quark masses in vacuum. In the third step, the divergent mass term is simultaneously absorbed by renormalizing the coupling constants in the mesonic sector, as was done when deriving the thermodynamic potential Ω_{PQM} in (7). And in the forth step, the divergent integral is renormalized by following dimensional regularization with the condition that it vanishes for all q^2 in the vacuum. Similarly, the polarization function of π^0

is

$$\begin{aligned}
\Pi_{\hat{\pi}^0}(iq_4, \mathbf{q}) &= \Pi_{\hat{\pi}^0}^v - \frac{3g_m^2}{4} \sum_{f=u,d} \int \frac{d^3\mathbf{k}}{(2\pi)^3} \sum_{u,t=\pm} \frac{-u t E_{\mathbf{k}+u\mathbf{q}/2}^f(iq_4) - u \mathbf{q} \cdot \mathbf{k} - \mathbf{q}^2/2}{E_{\mathbf{k}+u\mathbf{q}/2}^f [2u t E_{\mathbf{k}+u\mathbf{q}/2}^f(iq_4) + 2u \mathbf{q} \cdot \mathbf{k} + (iq_4)^2]} [LH_f^{ut} + 2L(H_f^{ut})^2 + (H_f^{ut})^3] F_f^{ut}, \\
\Pi_{\hat{\pi}^0}^v(q^2) &\equiv -\frac{3g_m^2}{2} \sum_{f=u,d} \int \frac{d^4k}{(2\pi)^4} \frac{-k \cdot (k+q) + m_f^2}{[-k^2 + m_f^2][-(k+q)^2 + m_f^2]} \Rightarrow -\frac{3g_m^2}{4} q^2 \sum_{f=u,d} \int \frac{d^4k}{(2\pi)^4} \frac{1}{[-k^2 + m_f^2][-(k+q)^2 + m_f^2]} \\
&= \frac{3g_m^2}{2(4\pi)^2} q^2 \sum_{f=u,d} \left(\ln \frac{m_f}{m_{f0}} + \sqrt{1 - 4 \frac{m_f^2}{q^2}} \operatorname{arccoth} \sqrt{1 - 4 \frac{m_f^2}{q^2}} - \sqrt{1 - 4 \frac{m_{f0}^2}{q^2}} \operatorname{arccoth} \sqrt{1 - 4 \frac{m_{f0}^2}{q^2}} \right). \quad (\text{A3})
\end{aligned}$$

The polarization functions of π^+ , K^0 and K^+ are a little different as the corresponding quark loops involve different flavors. Take $\Pi_{\hat{\pi}^+}$ for example, the polarization function can be evaluated as the following:

$$\begin{aligned}
\Pi_{\hat{\pi}^+}(iQ_4, \mathbf{q}) &= \Pi_{\hat{\pi}^+}^v - g_m^2 \sum_{c=r,g,b} \int \frac{d^3\mathbf{k}}{(2\pi)^3} \sum_{t=\pm} \frac{-E_{\mathbf{k}}^d(E_{\mathbf{k}}^d - t(iQ_4)) + (\mathbf{k} + \mathbf{q}) \cdot \mathbf{k} + m_u m_d}{E_{\mathbf{k}}^d [(E_{\mathbf{k}}^d - t(iQ_4))^2 - (\mathbf{k} + \mathbf{q})^2 - m_u^2]} \frac{1}{1 + e^{[E_{\mathbf{k}}^d - t(iq_c T + Q_d \mu_Q + \frac{\mu_B}{3})]/T}} \\
&\quad - g_m^2 \sum_{c=r,g,b} \int \frac{d^3\mathbf{k}}{(2\pi)^3} \sum_{t=\pm} \frac{-E_{\mathbf{k}}^u(E_{\mathbf{k}}^u + t(iQ_4)) + (\mathbf{k} - \mathbf{q}) \cdot \mathbf{k} + m_u m_d}{E_{\mathbf{k}}^u [(E_{\mathbf{k}}^u + t(iQ_4))^2 - (\mathbf{k} - \mathbf{q})^2 - m_d^2]} \frac{1}{1 + e^{[E_{\mathbf{k}}^u - t(iq_c T + Q_u \mu_Q + \frac{\mu_B}{3})]/T}} \\
&= \Pi_{\hat{\pi}^+}^v - 3g_m^2 \int \frac{d^3\mathbf{k}}{(2\pi)^3} \sum_{t=\pm} \frac{-E_{\mathbf{k}}^d(E_{\mathbf{k}}^d - t(iQ_4)) + (\mathbf{k} + \mathbf{q}) \cdot \mathbf{k} + m_u m_d}{E_{\mathbf{k}}^d [(E_{\mathbf{k}}^d - t(iQ_4))^2 - (\mathbf{k} + \mathbf{q})^2 - m_u^2]} [LH_d^t + 2L(H_d^t)^2 + (H_d^t)^3] F_d^t \\
&\quad - 3g_m^2 \int \frac{d^3\mathbf{k}}{(2\pi)^3} \sum_{t=\pm} \frac{-E_{\mathbf{k}}^u(E_{\mathbf{k}}^u + t(iQ_4)) + (\mathbf{k} - \mathbf{q}) \cdot \mathbf{k} + m_u m_d}{E_{\mathbf{k}}^u [(E_{\mathbf{k}}^u + t(iQ_4))^2 - (\mathbf{k} - \mathbf{q})^2 - m_d^2]} [LH_u^t + 2L(H_u^t)^2 + (H_u^t)^3] F_u^t \\
&= \Pi_{\hat{\pi}^+}^v - 3g_m^2 \int \frac{d^3\mathbf{k}}{(2\pi)^3} \sum_{t=\pm} \frac{[t E_{\mathbf{k}}^d(iQ_4) + \mathbf{q} \cdot \mathbf{k} - m_d(m_d - m_u)] [LH_d^t + 2L(H_d^t)^2 + (H_d^t)^3] F_d^t}{E_{\mathbf{k}}^d [-2t E_{\mathbf{k}}^d(iQ_4) - 2\mathbf{q} \cdot \mathbf{k} + (iQ_4)^2 - \mathbf{q}^2 - m_u^2 + m_d^2]} \\
&\quad - 3g_m^2 \int \frac{d^3\mathbf{k}}{(2\pi)^3} \sum_{t=\pm} \frac{[-t E_{\mathbf{k}}^u(iQ_4) - \mathbf{q} \cdot \mathbf{k} - m_u(m_u - m_d)] [LH_u^t + 2L(H_u^t)^2 + (H_u^t)^3] F_u^t}{E_{\mathbf{k}}^u [2t E_{\mathbf{k}}^u(iQ_4) + 2\mathbf{q} \cdot \mathbf{k} + (iQ_4)^2 - \mathbf{q}^2 - m_d^2 + m_u^2]}, \quad (\text{A4})
\end{aligned}$$

where the vacuum term is renormalized in the following way:

$$\begin{aligned}
\Pi_{\hat{\pi}^+}^v(Q^2) &\equiv -6g_m^2 \int \frac{d^4k}{(2\pi)^4} \frac{-k \cdot (k+Q) + m_d m_u}{[-k^2 + m_d^2][-(k+Q)^2 + m_u^2]} \\
&= -6g_m^2 \int \frac{d^4k}{(2\pi)^4} \frac{1}{[-k^2 + m_d^2]} - 3g_m^2 [Q^2 - (m_d - m_u)^2] \int \frac{d^4k}{(2\pi)^4} \frac{1}{[-k^2 + m_d^2][-(k+Q)^2 + m_u^2]} \\
&\Rightarrow -3g_m^2 [Q^2 - (m_d - m_u)^2] \int \frac{d^4k}{(2\pi)^4} \frac{1}{[-k^2 + m_d^2][-(k+Q)^2 + m_u^2]} \\
&= \frac{3g_m^2}{(4\pi)^2} [Q^2 - (m_d - m_u)^2] \left[\ln m_d m_u + \frac{m_d^2 - m_u^2}{Q^2} \ln \frac{m_d}{m_u} + M_{du}^+ M_{du}^- \ln \left| \frac{M_{du}^+ + M_{du}^-}{M_{du}^+ - M_{du}^-} \right| - (m_f \rightarrow m_{f0}) \right] (\text{A5})
\end{aligned}$$

with $Q \equiv (Q_4, \mathbf{q})$ and $M_{f_1 f_2}^\pm \equiv \sqrt{1 - \frac{(m_{f_1} \pm m_{f_2})^2}{Q^2}}$. In the limit $m_u \rightarrow m_d$ and $\mu_Q = 0$, $\Pi_{\hat{\pi}^+}^v \rightarrow 2\Pi_{\hat{\pi}^0}^v$ and the degeneracy between $\hat{\pi}^+$ and $\hat{\pi}^0$ is well reproduced for the vacuum and thermal parts.

The polarization functions of K^0 and K^+ can be simply obtained by changing the subscript u to s and d to s from

$\Pi_{\hat{\pi}^+}$, respectively. We have

$$\begin{aligned}
\Pi_{\hat{K}^0}(iq_4, \mathbf{q}) &= \frac{3g_m^2}{(4\pi)^2} [q^2 - (m_d - m_s)^2] \left[\ln m_d m_s + \frac{m_d^2 - m_s^2}{q^2} \ln \frac{m_d}{m_s} + M_{ds}^+ M_{ds}^- \ln \left| \frac{M_{ds}^+ + M_{ds}^-}{M_{ds}^+ - M_{ds}^-} \right| - (m_f \rightarrow m_{f0}) \right] \\
&\quad - 3g_m^2 \int \frac{d^3 \mathbf{k}}{(2\pi)^3} \sum_{t=\pm} \frac{t E_{\mathbf{k}}^s(iq_4) + \mathbf{q} \cdot \mathbf{k} - m_s(m_s - m_d)}{E_{\mathbf{k}}^s[-2t E_{\mathbf{k}}^s(iq_4) - 2\mathbf{q} \cdot \mathbf{k} + (iq_4)^2 - \mathbf{q}^2 - m_d^2 + m_s^2]} [LH_s^t + 2L(H_s^t)^2 + (H_s^t)^3] F_s^t \\
&\quad - 3g_m^2 \int \frac{d^3 \mathbf{k}}{(2\pi)^3} \sum_{t=\pm} \frac{-t E_{\mathbf{k}}^d(iq_4) - \mathbf{q} \cdot \mathbf{k} + m_d(m_s - m_d)}{E_{\mathbf{k}}^d[2t E_{\mathbf{k}}^d(iq_4) + 2\mathbf{q} \cdot \mathbf{k} + (iq_4)^2 - \mathbf{q}^2 + m_d^2 - m_s^2]} [LH_d^t + 2L(H_d^t)^2 + (H_d^t)^3] F_d^t \quad (A6) \\
\Pi_{\hat{K}^+}(iQ_4, \mathbf{q}) &= \frac{3g_m^2}{(4\pi)^2} [Q^2 - (m_u - m_s)^2] \left[\ln m_u m_s + \frac{m_u^2 - m_s^2}{Q^2} \ln \frac{m_u}{m_s} + M_{us}^+ M_{us}^- \ln \left| \frac{M_{us}^+ + M_{us}^-}{M_{us}^+ - M_{us}^-} \right| - (m_f \rightarrow m_{f0}) \right] \\
&\quad - 3g_m^2 \int \frac{d^3 \mathbf{k}}{(2\pi)^3} \sum_{t=\pm} \frac{[t E_{\mathbf{k}}^s(iQ_4) + \mathbf{q} \cdot \mathbf{k} - m_s(m_s - m_u)] [LH_s^t + 2L(H_s^t)^2 + (H_s^t)^3] F_s^t}{E_{\mathbf{k}}^s[-2t E_{\mathbf{k}}^s(iQ_4) - 2\mathbf{q} \cdot \mathbf{k} + (iQ_4)^2 - \mathbf{q}^2 - m_u^2 + m_s^2]} \\
&\quad - 3g_m^2 \int \frac{d^3 \mathbf{k}}{(2\pi)^3} \sum_{t=\pm} \frac{[-t E_{\mathbf{k}}^u(iQ_4) - \mathbf{q} \cdot \mathbf{k} + m_u(m_s - m_u)] [LH_u^t + 2L(H_u^t)^2 + (H_u^t)^3] F_u^t}{E_{\mathbf{k}}^u[2t E_{\mathbf{k}}^u(iQ_4) + 2\mathbf{q} \cdot \mathbf{k} + (iQ_4)^2 - \mathbf{q}^2 + m_u^2 - m_s^2]}. \quad (A7)
\end{aligned}$$

Note that as we have set the component quark masses different for π^+ , K^0 and K^+ a priori, the momentum integral in one branch can be shifted by \mathbf{q} without changing the results. However, there are no mass differences in the denominators of the integrands for σ and π^0 , thus such a momentum shift could cause ambiguity when one expands the integrand around $|\mathbf{q}| \sim 0$.

For a large $|\mathbf{q}|$, the momentum shift is valid for all mesons, so we will take $\hat{\pi}^+$ for example to show the general features of the polarization functions in such a limit. For the static case with $iQ_4 = 0$, the leading contribution of the vacuum term is $\Pi_{\hat{\pi}^+}^v(-|\mathbf{q}|^2) = \frac{3g_m^2}{(4\pi)^2} (m_{d0}^2 + m_{u0}^2 - m_d^2 - m_u^2) \ln |\mathbf{q}|^2$. And the thermal term vanishes for two facts: The integrals around large k are greatly suppressed due to the presence of H_f^t , and the denominator is of order $o(|\mathbf{q}|^2)$ compared to the numerator of order $o(|\mathbf{q}|)$. To study the pole energy, we take the continuation $iQ_4 \rightarrow -q_0$, and then we will find the polarization function to be a constant by setting $q_0^2 - |\mathbf{q}|^2 = m_{\hat{\pi}^+}^2$, that is,

$$\Pi_{\hat{\pi}^+}(m_{\hat{\pi}^+}^2) = \Pi_{\hat{\pi}^+}^v(m_{\hat{\pi}^+}^2) + 3g_m^2 \int \frac{d^3 \mathbf{k}}{(2\pi)^3} \sum_{f=u,d}^{t=\pm} \frac{1}{2E_{\mathbf{k}}^f} [LH_f^t + 2L(H_f^t)^2 + (H_f^t)^3] F_f^t. \quad (A8)$$

Note that the thermal term is independent of $m_{\hat{\pi}^+}^2$ and completely controlled by the physical parameters T, μ_B and μ_Q . The effective mass $m_{\hat{\pi}^+}$ can be calculated self-consistently from the pole equation, $-m_{\hat{\pi}^+}^2 + \tilde{m}_{\hat{\pi}^+}^2 + \Pi_{\hat{\pi}^+}(m_{\hat{\pi}^+}^2) = 0$, but is not important in the large $|\mathbf{q}|$ limit. In summary, the polarization functions of all the mesons show two general features in the large $|\mathbf{q}|$ limit: proportional to $\ln |\mathbf{q}|^2$ in the static case and $|\mathbf{q}|$ -independent for $q_0^2 - |\mathbf{q}|^2 = m_{\hat{\pi}^+}^2$.

Appendix B: Small momentum expansion of polarization functions

At finite temperature and density, the system is isotropic, so all the polarization functions should depend on the magnitude rather than the direction of \mathbf{q} . For $\hat{\sigma}$ meson, after setting $iq_4 = 0$, one can obtain around $\mathbf{q}^2 = 0$:

$$\begin{aligned}
\Pi_{\hat{\sigma}} &\approx -\frac{6g_m^2}{(4\pi)^2} \sum_{f=u,d} m_f^2 \ln \frac{m_f}{m_{f0}} - \frac{3g_m^2}{2(4\pi)^2} \mathbf{q}^2 \sum_{f=u,d} \left[\ln \frac{m_f}{m_{f0}} + \frac{1}{3} \left(1 - \frac{m_f^2}{m_{f0}^2} \right) \right] + \frac{3g_m^2}{16} \sum_{f=u,d} (\mathbf{q}^2 + 4m_f^2) \sum_{t=\pm} Q_f^t(\mathbf{q}^2) \\
&\quad + \frac{3g_m^2}{4} \sum_{f=u,d} \int \frac{d^3 \mathbf{k}}{(2\pi)^3} \sum_{t=\pm} \frac{1}{E_{\mathbf{k}}^f} [LH_f^t + 2L(H_f^t)^2 + (H_f^t)^3] F_f^t. \quad (B1)
\end{aligned}$$

Here, the momentum expansion of the thermal parts can be evaluated as

$$Q_f^t(\mathbf{q}^2) \equiv \int \frac{d^3 \mathbf{k}}{(2\pi)^3} \sum_{u=\pm} \frac{u}{E_{\mathbf{k}+u\mathbf{q}/2}^f} [LH_f^{ut} + 2L(H_f^{ut})^2 + (H_f^{ut})^3] F_f^{ut} \approx Q_f^{t(0)} + Q_f^{t(2)} \mathbf{q}^2 \quad (B2)$$

with the leading and quadratic coefficients

$$\begin{aligned}
Q_f^{t(0)} &= 2 \int \frac{d^3\mathbf{k}}{(2\pi)^3} \frac{\partial}{\partial(\mathbf{k}^2)} \frac{1}{E_{\mathbf{k}}^f} [LH_f^t + 2L(H_f^t)^2 + (H_f^t)^3] F_f^t = - \int_0^\infty \frac{dk}{2\pi^2} \frac{1}{E_{\mathbf{k}}^f} [LH_f^t + 2L(H_f^t)^2 + (H_f^t)^3] F_f^t, \\
Q_f^{t(2)} &= \int \frac{d^3\mathbf{k}}{(2\pi)^3} \left[\frac{1}{2} \frac{\partial^2}{\partial(\mathbf{k}^2)^2} + (\hat{\mathbf{q}} \cdot \mathbf{k})^2 \frac{1}{3} \frac{\partial^3}{\partial(\mathbf{k}^2)^3} \right] \frac{1}{E_{\mathbf{k}}^f} [LH_f^t + 2L(H_f^t)^2 + (H_f^t)^3] F_f^t \\
&= \int \frac{d^3\mathbf{k}}{(2\pi)^3} \left[\frac{1}{2} \frac{\partial^2}{\partial(\mathbf{k}^2)^2} + \frac{\mathbf{k}^2}{9} \frac{\partial^3}{\partial(\mathbf{k}^2)^3} \right] \frac{1}{E_{\mathbf{k}}^f} [LH_f^t + 2L(H_f^t)^2 + (H_f^t)^3] F_f^t \\
&= \int_0^\infty \frac{k^2 dk}{6\pi^2} \frac{\partial^2}{\partial(k^2)^2} \frac{1}{E_{\mathbf{k}}^f} [LH_f^t + 2L(H_f^t)^2 + (H_f^t)^3] F_f^t = - \int_0^\infty \frac{dk}{12\pi^2} \frac{\partial}{\partial(k^2)} \frac{1}{E_{\mathbf{k}}^f} [LH_f^t + 2L(H_f^t)^2 + (H_f^t)^3] F_f^t \\
&= - \int_0^\infty \frac{dk}{24\pi^2 k^2} \left\{ \frac{1}{E_{\mathbf{k}}^f} [LH_f^t + 2L(H_f^t)^2 + (H_f^t)^3] F_f^t - (\mathbf{k} \rightarrow 0) \right\}. \tag{B3}
\end{aligned}$$

That for $\hat{\pi}^0$ follows directly as

$$\Pi_{\hat{\pi}^0} \approx - \frac{3g_m^2}{2(4\pi)^2} \mathbf{q}^2 \sum_{f=u,d} \ln \frac{m_f}{m_{f0}} + \frac{3g_m^2}{16} \mathbf{q}^2 \sum_{f=u,d} \sum_{t=\pm} Q_f^{t(0)} + \frac{3g_m^2}{4} \sum_{f=u,d} \int \frac{d^3\mathbf{k}}{(2\pi)^3} \sum_{t=\pm} \frac{1}{E_{\mathbf{k}}^f} [LH_f^t + 2L(H_f^t)^2 + (H_f^t)^3] F_f^t \tag{B4}$$

Similarly, for $\hat{\pi}^+$, after setting $iQ_4 = 0$, one can obtain around $\mathbf{q}^2 = 0$:

$$\begin{aligned}
\Pi_{\hat{\pi}^+} &= - \frac{3g_m^2}{(4\pi)^2} [\mathbf{q}^2 + (m_d - m_u)^2] \left[\ln m_d m_u + \frac{m_d^2 + m_u^2}{m_d^2 - m_u^2} \ln \frac{m_d}{m_u} + \mathbf{q}^2 \frac{m_d^4 - m_u^4 - 4m_d^2 m_u^2 \ln \frac{m_d}{m_u}}{2(m_d^2 - m_u^2)^3} - (m_f \rightarrow m_{f0}) \right] \\
&\quad + \frac{3g_m^2}{2} [\mathbf{q}^2 + (m_d - m_u)^2] \sum_{t=\pm} \sum_{f=u,d} Q_{\hat{\pi}^+f}^t(\mathbf{q}^2) + \frac{3g_m^2}{2} \sum_{f=u,d} \int \frac{d^3\mathbf{k}}{(2\pi)^3} \sum_{t=\pm} \frac{1}{E_{\mathbf{k}}^f} [LH_f^t + 2L(H_f^t)^2 + (H_f^t)^3] F_f^t \tag{B5}
\end{aligned}$$

Here, the momentum expansion of the thermal parts can be evaluated as

$$\begin{aligned}
Q_{\hat{\pi}^+d}^t(\mathbf{q}^2) &= \int \frac{d^3\mathbf{k}}{(2\pi)^3} \frac{1}{E_{\mathbf{k}}^d [-2\mathbf{q} \cdot \mathbf{k} - q^2 - m_u^2 + m_d^2]} [LH_d^t + 2L(H_d^t)^2 + (H_d^t)^3] F_d^t \\
&= \int_0^\infty \frac{dk}{2(2\pi)^2} \frac{1}{E_{\mathbf{k}}^d} \frac{k}{q} \ln \left| \frac{-2qk + q^2 + m_u^2 - m_d^2}{2qk + q^2 + m_u^2 - m_d^2} \right| [LH_d^t + 2L(H_d^t)^2 + (H_d^t)^3] F_d^t \approx Q_{\hat{\pi}^+d}^{t(0)} + Q_{\hat{\pi}^+d}^{t(2)} \mathbf{q}^2; \tag{B6}
\end{aligned}$$

$$\begin{aligned}
Q_{\hat{\pi}^+u}^t(\mathbf{q}^2) &= \int \frac{d^3\mathbf{k}}{(2\pi)^3} \frac{1}{E_{\mathbf{k}}^u [2\mathbf{q} \cdot \mathbf{k} - q^2 + m_u^2 - m_d^2]} [LH_u^t + 2L(H_u^t)^2 + (H_u^t)^3] F_u^t \\
&= \int_0^\infty \frac{dk}{2(2\pi)^2} \frac{1}{E_{\mathbf{k}}^u} \frac{k}{q} \ln \left| \frac{2qk - q^2 + m_u^2 - m_d^2}{-2qk - q^2 + m_u^2 - m_d^2} \right| [LH_u^t + 2L(H_u^t)^2 + (H_u^t)^3] F_u^t \approx Q_{\hat{\pi}^+u}^{t(0)} + Q_{\hat{\pi}^+u}^{t(2)} \mathbf{q}^2 \tag{B7}
\end{aligned}$$

with the leading and quadratic coefficients

$$Q_{\hat{\pi}^+d}^{t(0)} = - \frac{1}{m_u^2 - m_d^2} \int_0^\infty \frac{2k^2 dk}{(2\pi)^2} \frac{1}{E_{\mathbf{k}}^d} [LH_d^t + 2L(H_d^t)^2 + (H_d^t)^3] F_d^t, \tag{B8}$$

$$Q_{\hat{\pi}^+d}^{t(2)} = \frac{1}{3(m_u^2 - m_d^2)^3} \int_0^\infty \frac{2k^2 dk}{(2\pi)^2} \frac{3(m_u^2 - m_d^2) - 4k^2}{E_{\mathbf{k}}^d} [LH_d^t + 2L(H_d^t)^2 + (H_d^t)^3] F_d^t; \tag{B9}$$

$$Q_{\hat{\pi}^+u}^{t(0)} = \frac{1}{m_u^2 - m_d^2} \int_0^\infty \frac{2k^2 dk}{(2\pi)^2} \frac{1}{E_{\mathbf{k}}^u} [LH_u^t + 2L(H_u^t)^2 + (H_u^t)^3] F_u^t, \tag{B10}$$

$$Q_{\hat{\pi}^+u}^{t(2)} = \frac{1}{3(m_u^2 - m_d^2)^3} \int_0^\infty \frac{2k^2 dk}{(2\pi)^2} \frac{3(m_u^2 - m_d^2) + 4k^2}{E_{\mathbf{k}}^u} [LH_u^t + 2L(H_u^t)^2 + (H_u^t)^3] F_u^t. \tag{B11}$$

By utilizing partial integral, one can check that

$$\lim_{m_u \rightarrow m_d} [\mathbf{q}^2 + (m_d - m_u)^2] \sum_{f=u,d} Q_{\hat{\pi}^+f}^t(\mathbf{q}^2) = \mathbf{q}^2 \lim_{m_u \rightarrow m_d} \sum_{f=u,d} Q_{\hat{\pi}^+f}^{t(0)} = \frac{\mathbf{q}^2}{4} \sum_{f=u,d} Q_f^{t(0)} \tag{B12}$$

up to $o(\mathbf{q}^2)$ for $\mu_Q = 0$, thus π^+ is degenerate with π^0 in the limit $m_u = m_d$ as should be.

By changing the subscripts, those of K^0 and K^+ can be directly obtained as

$$\begin{aligned} \Pi_{\hat{K}^0} = & -\frac{3g_m^2}{(4\pi)^2} [\mathbf{q}^2 + (m_d - m_s)^2] \left[\ln m_d m_s + \frac{m_d^2 + m_s^2}{m_d^2 - m_s^2} \ln \frac{m_d}{m_s} + \mathbf{q}^2 \frac{m_d^4 - m_s^4 - 4m_d^2 m_s^2 \ln \frac{m_d}{m_s}}{2(m_d^2 - m_s^2)^3} - (m_f \rightarrow m_{f0}) \right] \\ & + \frac{3g_m^2}{2} [\mathbf{q}^2 + (m_d - m_s)^2] \sum_{t=\pm} \sum_{f=s,d} [Q_{\hat{K}^0 f}^{t(0)} + Q_{\hat{K}^0 f}^{t(2)} \mathbf{q}^2] + \frac{3g_m^2}{2} \sum_{f=s,d} \int \frac{d^3 \mathbf{k}}{(2\pi)^3} \sum_{t=\pm} \frac{1}{E_{\mathbf{k}}^f} [LH_f^t + 2L(H_f^t)^2 + (H_f^t)^3] F_f^t \end{aligned} \quad (\text{B13})$$

$$\begin{aligned} \Pi_{\hat{K}^+} = & -\frac{3g_m^2}{(4\pi)^2} [\mathbf{q}^2 + (m_s - m_u)^2] \left[\ln m_s m_u + \frac{m_s^2 + m_u^2}{m_s^2 - m_u^2} \ln \frac{m_s}{m_u} + \mathbf{q}^2 \frac{m_s^4 - m_u^4 - 4m_s^2 m_u^2 \ln \frac{m_s}{m_u}}{2(m_s^2 - m_u^2)^3} - (m_f \rightarrow m_{f0}) \right] \\ & + \frac{3g_m^2}{2} [\mathbf{q}^2 + (m_s - m_u)^2] \sum_{t=\pm} \sum_{f=u,s} [Q_{\hat{K}^+ f}^{t(0)} + Q_{\hat{K}^+ f}^{t(2)} \mathbf{q}^2] + \frac{3g_m^2}{2} \sum_{f=u,s} \int \frac{d^3 \mathbf{k}}{(2\pi)^3} \sum_{t=\pm} \frac{1}{E_{\mathbf{k}}^f} [LH_f^t + 2L(H_f^t)^2 + (H_f^t)^3] F_f^t \end{aligned} \quad (\text{B14})$$

with the leading and quadratic expansion coefficients of the thermal parts

$$Q_{\hat{K}^0 d}^{t(0)} = -\frac{1}{m_s^2 - m_d^2} \int_0^\infty \frac{2k^2 dk}{(2\pi)^2} \frac{1}{E_{\mathbf{k}}^d} [LH_d^t + 2L(H_d^t)^2 + (H_d^t)^3] F_d^t, \quad (\text{B15})$$

$$Q_{\hat{K}^0 d}^{t(2)} = \frac{1}{3(m_s^2 - m_d^2)^3} \int_0^\infty \frac{2k^2 dk}{(2\pi)^2} \frac{3(m_s^2 - m_d^2) - 4k^2}{E_{\mathbf{k}}^d} [LH_d^t + 2L(H_d^t)^2 + (H_d^t)^3] F_d^t; \quad (\text{B16})$$

$$Q_{\hat{K}^0 s}^{t(0)} = \frac{1}{m_s^2 - m_d^2} \int_0^\infty \frac{2k^2 dk}{(2\pi)^2} \frac{1}{E_{\mathbf{k}}^s} [LH_s^t + 2L(H_s^t)^2 + (H_s^t)^3] F_s^t, \quad (\text{B17})$$

$$Q_{\hat{K}^0 s}^{t(2)} = \frac{1}{3(m_s^2 - m_d^2)^3} \int_0^\infty \frac{2k^2 dk}{(2\pi)^2} \frac{3(m_s^2 - m_d^2) + 4k^2}{E_{\mathbf{k}}^s} [LH_s^t + 2L(H_s^t)^2 + (H_s^t)^3] F_s^t; \quad (\text{B18})$$

$$Q_{\hat{K}^+ s}^{t(0)} = -\frac{1}{m_u^2 - m_s^2} \int_0^\infty \frac{2k^2 dk}{(2\pi)^2} \frac{1}{E_{\mathbf{k}}^s} [LH_s^t + 2L(H_s^t)^2 + (H_s^t)^3] F_s^t, \quad (\text{B19})$$

$$Q_{\hat{K}^+ s}^{t(2)} = \frac{1}{3(m_u^2 - m_s^2)^3} \int_0^\infty \frac{2k^2 dk}{(2\pi)^2} \frac{3(m_u^2 - m_s^2) - 4k^2}{E_{\mathbf{k}}^s} [LH_s^t + 2L(H_s^t)^2 + (H_s^t)^3] F_s^t; \quad (\text{B20})$$

$$Q_{\hat{K}^+ u}^{t(0)} = \frac{1}{m_u^2 - m_s^2} \int_0^\infty \frac{2k^2 dk}{(2\pi)^2} \frac{1}{E_{\mathbf{k}}^u} [LH_u^t + 2L(H_u^t)^2 + (H_u^t)^3] F_u^t, \quad (\text{B21})$$

$$Q_{\hat{K}^+ u}^{t(2)} = \frac{1}{3(m_u^2 - m_s^2)^3} \int_0^\infty \frac{2k^2 dk}{(2\pi)^2} \frac{3(m_u^2 - m_s^2) + 4k^2}{E_{\mathbf{k}}^u} [LH_u^t + 2L(H_u^t)^2 + (H_u^t)^3] F_u^t. \quad (\text{B22})$$

Eventually, for the static case, the wave function renormalizations in front of \mathbf{q}^2 can be summarized as

$$Z_{\sigma}^{\perp} = 1 - \frac{3g_m^2}{(4\pi)^2} \sum_{f=u,d} \left[\ln \frac{m_f}{m_{f0}} + \frac{1}{3} \left(1 - \frac{m_f^2}{m_{f0}^2} \right) \right] + \frac{3g_m^2}{8} \sum_{f=u,d} \sum_{t=\pm} [Q_f^{t(0)} + 4m_f^2 Q_f^{t(2)}], \quad (\text{B23})$$

$$Z_{\pi^0}^{\perp} = 1 - \frac{3g_m^2}{(4\pi)^2} \sum_{f=u,d} \ln \frac{m_f}{m_{f0}} + \frac{3g_m^2}{8} \sum_{f=u,d} \sum_{t=\pm} Q_f^{t(0)}, \quad (\text{B24})$$

$$Z_{\pi^+}^{\perp} = 1 - \frac{3g_m^2}{(4\pi)^2} \left[\ln \frac{m_d m_u}{m_{d0} m_{u0}} + \frac{m_d^2 + m_u^2}{m_d^2 - m_u^2} \ln \frac{m_d}{m_u} - \frac{m_{d0}^2 + m_{u0}^2}{m_{d0}^2 - m_{u0}^2} \ln \frac{m_{d0}}{m_{u0}} + (m_d - m_u)^2 \left(\frac{m_d^4 - m_u^4 - 4m_d^2 m_u^2 \ln \frac{m_d}{m_u}}{2(m_d^2 - m_u^2)^3} - \frac{m_{d0}^4 - m_{u0}^4 - 4m_{d0}^2 m_{u0}^2 \ln \frac{m_{d0}}{m_{u0}}}{2(m_{d0}^2 - m_{u0}^2)^3} \right) \right] + \frac{3g_m^2}{2} \sum_{t=\pm} \sum_{f=u,d} [Q_{\pi^+f}^{t(0)} + (m_d - m_u)^2 Q_{\pi^+f}^{t(2)}], \quad (\text{B25})$$

$$Z_{\bar{K}^0}^{\perp} = 1 - \frac{3g_m^2}{(4\pi)^2} \left[\ln \frac{m_d m_s}{m_{d0} m_{s0}} + \frac{m_d^2 + m_s^2}{m_d^2 - m_s^2} \ln \frac{m_d}{m_s} - \frac{m_{d0}^2 + m_{s0}^2}{m_{d0}^2 - m_{s0}^2} \ln \frac{m_{d0}}{m_{s0}} + (m_d - m_s)^2 \left(\frac{m_d^4 - m_s^4 - 4m_d^2 m_s^2 \ln \frac{m_d}{m_s}}{2(m_d^2 - m_s^2)^3} - \frac{m_{d0}^4 - m_{s0}^4 - 4m_{d0}^2 m_{s0}^2 \ln \frac{m_{d0}}{m_{s0}}}{2(m_{d0}^2 - m_{s0}^2)^3} \right) \right] + \frac{3g_m^2}{2} \sum_{t=\pm} \sum_{f=s,d} [Q_{\bar{K}^0f}^{t(0)} + (m_d - m_s)^2 Q_{\bar{K}^0f}^{t(2)}], \quad (\text{B26})$$

$$Z_{\bar{K}^+}^{\perp} = 1 - \frac{3g_m^2}{(4\pi)^2} \left[\ln \frac{m_s m_u}{m_{s0} m_{u0}} + \frac{m_s^2 + m_u^2}{m_s^2 - m_u^2} \ln \frac{m_s}{m_u} - \frac{m_{s0}^2 + m_{u0}^2}{m_{s0}^2 - m_{u0}^2} \ln \frac{m_{s0}}{m_{u0}} + (m_s - m_u)^2 \left(\frac{m_s^4 - m_u^4 - 4m_s^2 m_u^2 \ln \frac{m_s}{m_u}}{2(m_s^2 - m_u^2)^3} - \frac{m_{s0}^4 - m_{u0}^4 - 4m_{s0}^2 m_{u0}^2 \ln \frac{m_{s0}}{m_{u0}}}{2(m_{s0}^2 - m_{u0}^2)^3} \right) \right] + \frac{3g_m^2}{2} \sum_{t=\pm} \sum_{f=u,s} [Q_{\bar{K}^+f}^{t(0)} + (m_s - m_u)^2 Q_{\bar{K}^+f}^{t(2)}]. \quad (\text{B27})$$

Note that $Q_f^{t(0)}$ would diverge around the infrared integral region $k \sim 0$ in the limit $m_f \rightarrow 0$, and the degree of divergence can be estimated by taking Taylor expansion around $E_{\mathbf{k}}^f \sim 0$ as following

$$\sum_{t=\pm} Q_f^{t(0)} \sim \int_0^{\Lambda} \frac{dk}{2(2\pi)^2} \frac{1}{E_{\mathbf{k}}^f} \sim -\frac{1}{2(2\pi)^2} \log m_f. \quad (\text{B28})$$

Then, in chiral limit, the thermal part would induce a negatively divergent correction to the wave function renormalization when chiral symmetry is fully restored. Thus, the moat boundaries of σ and π mesons would be exactly the same as the chiral transition line if there are no contributions from vacuum polarizations. By taking the vacuum polarizations into account, one would find that the logarithmic divergences exactly cancel out, and the moat boundaries are not necessarily locked to the chiral transition line.

-
- | | |
|--|--|
| <p>[1] C. F. von Weizsacker, The theory of nuclear masses, <i>Z. Physik</i>, 96: 431 (1935).</p> <p>[2] B. A. Li, L. W. Chen and C. M. Ko, “Recent Progress and New Challenges in Isospin Physics with Heavy-Ion Reactions,” <i>Phys. Rept.</i> 464, 113-281 (2008).</p> <p>[3] A. E. S. Green and D. F. Edwards, “Discontinuities in the Nuclear Mass Surface,” <i>Phys. Rev.</i> 91, 46-53 (1953).</p> <p>[4] A. E. S. Green, “Coulomb Radius Constant from Nuclear Masses,” <i>Phys. Rev.</i> 95, 1006-1009 (1954).</p> <p>[5] T. D. Lee and G. C. Wick, “Vacuum Stability and Vacuum Excitation in a Spin 0 Field Theory,” <i>Phys. Rev. D</i> 9, 2291-2316 (1974).</p> <p>[6] R. Bellwied, S. Borsanyi, Z. Fodor, J. Günther, S. D. Katz, C. Ratti and K. K. Szabo, “The QCD phase diagram from analytic continuation,” <i>Phys. Lett. B</i> 751, 559-564 (2015).</p> | <p>[7] A. Bazavov <i>et al.</i> [HotQCD], “Chiral crossover in QCD at zero and non-zero chemical potentials,” <i>Phys. Lett. B</i> 795, 15-21 (2019).</p> <p>[8] A. Andronic, P. Braun-Munzinger, K. Redlich and J. Stachel, “Decoding the phase structure of QCD via particle production at high energy,” <i>Nature</i> 561, no.7723, 321-330 (2018).</p> <p>[9] L. Adamczyk <i>et al.</i> [STAR], “Bulk Properties of the Medium Produced in Relativistic Heavy-Ion Collisions from the Beam Energy Scan Program,” <i>Phys. Rev. C</i> 96, no.4, 044904 (2017).</p> <p>[10] X. Luo and N. Xu, “Search for the QCD Critical Point with Fluctuations of Conserved Quantities in Relativistic Heavy-Ion Collisions at RHIC : An Overview,” <i>Nucl. Sci. Tech.</i> 28, no.8, 112 (2017).</p> <p>[11] X. Luo, Q. Wang, N. Xu and P. Zhuang, “Properties of</p> |
|--|--|

- QCD Matter at High Baryon Density,” Springer, 2022, ISBN 978-981-19-4440-6, 978-981-19-4443-7, 978-981-19-4441-3.
- [12] W. j. Fu, J. M. Pawłowski and F. Rennecke, “QCD phase structure at finite temperature and density,” *Phys. Rev. D* **101**, no.5, 054032 (2020).
- [13] F. Gao and J. M. Pawłowski, “Chiral phase structure and critical end point in QCD,” *Phys. Lett. B* **820**, 136584 (2021).
- [14] P. J. Gunkel and C. S. Fischer, “Locating the critical endpoint of QCD: Mesonic backcoupling effects,” *Phys. Rev. D* **104**, no.5, 054022 (2021).
- [15] R. G. Cai, S. He, L. Li and Y. X. Wang, “Probing QCD critical point and induced gravitational wave by black hole physics,” *Phys. Rev. D* **106**, no.12, L121902 (2022).
- [16] A. Sorensen and P. Sorensen, “Locating the critical point for the hadron to quark-gluon plasma phase transition from finite-size scaling of proton cumulants in heavy-ion collisions,” [arXiv:2405.10278 [nucl-th]].
- [17] D. A. Clarke, P. Dimopoulos, F. Di Renzo, J. Goswami, C. Schmidt, S. Singh and K. Zambello, “Searching for the QCD critical endpoint using multi-point Padé approximations,” [arXiv:2405.10196 [hep-lat]].
- [18] L. McLerran and R. D. Pisarski, “Phases of cold, dense quarks at large $N(c)$,” *Nucl. Phys. A* **796**, 83-100 (2007).
- [19] K. Fukushima and T. Kojo, “The Quarkyonic Star,” *Astrophys. J.* **817**, no.2, 180 (2016).
- [20] L. McLerran and S. Reddy, “Quarkyonic Matter and Neutron Stars,” *Phys. Rev. Lett.* **122**, no. 12, 122701 (2019).
- [21] G. Cao and J. Liao, “A field theoretical model for quarkyonic matter,” *JHEP* **10**, 168 (2020).
- [22] G. Cao, “Quarkyonic matter state of neutron stars,” *Phys. Rev. D* **105**, no.11, 114020 (2022).
- [23] R. D. Pisarski and F. Rennecke, “Signatures of Moat Regimes in Heavy-Ion Collisions,” *Phys. Rev. Lett.* **127**, no.15, 152302 (2021).
- [24] F. Rennecke and R. D. Pisarski, “Moat Regimes in QCD and their Signatures in Heavy-Ion Collisions,” *PoS CPOD2021*, 016 (2022).
- [25] F. Rennecke, R. D. Pisarski and D. H. Rischke, “Particle interferometry in a moat regime,” *Phys. Rev. D* **107**, no.11, 116011 (2023).
- [26] W. j. Fu, J. M. Pawłowski, R. D. Pisarski, F. Rennecke, R. Wen and S. Yin, “The QCD moat regime and its real-time properties,” [arXiv:2412.15949 [hep-ph]].
- [27] S. Töpfel, J. M. Pawłowski and J. Braun, “Phase structure of quark matter and in-medium properties of mesons from Callan-Symanzik flows,” [arXiv:2412.16059 [hep-ph]].
- [28] B. J. Schaefer, M. Wagner and J. Wambach, “Thermodynamics of (2+1)-flavor QCD: Confronting Models with Lattice Studies,” *Phys. Rev. D* **81**, 074013 (2010).
- [29] C. Ratti, M. A. Thaler and W. Weise, “Phases of QCD: Lattice thermodynamics and a field theoretical model,” *Phys. Rev. D* **73**, 014019 (2006).
- [30] T. K. Herbst, J. M. Pawłowski and B. J. Schaefer, *Phys. Lett. B* **696**, 58-67 (2011).
- [31] B. J. Schaefer and M. Wagner, “The Three-flavor chiral phase structure in hot and dense QCD matter,” *Phys. Rev. D* **79**, 014018 (2009).